Accepted Manuscript

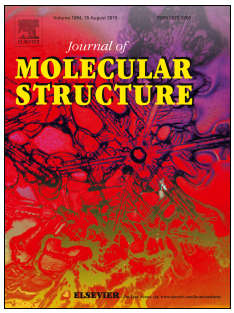

Synthesis, spectroscopic, structural elucidation, NLO characteristic and Hirshfeld surface analysis of (*E*)-1-(4-ethylphenyl)-3-(4-(heptyloxy) phenyl)prop-2-en-1-one: A dual approach of experimental and DFT calculations

Adibah Izzati Daud, Wan M. Khairul, Elccey Augustine, Suhana Arshad, Ibrahim Abdul Razak

PII: S0022-2860(19)30610-6

DOI: https://doi.org/10.1016/j.molstruc.2019.05.046

Reference: MOLSTR 26553

To appear in: *Journal of Molecular Structure*

Received Date: 22 January 2019

Revised Date: 12 May 2019

Accepted Date: 13 May 2019

Please cite this article as: A.I. Daud, W.M. Khairul, E. Augustine, S. Arshad, I.A. Razak, Synthesis, spectroscopic, structural elucidation, NLO characteristic and Hirshfeld surface analysis of (*E*)-1-(4-ethylphenyl)-3-(4-(heptyloxy) phenyl)prop-2-en-1-one: A dual approach of experimental and DFT calculations, *Journal of Molecular Structure* (2019), doi: https://doi.org/10.1016/j.molstruc.2019.05.046.

This is a PDF file of an unedited manuscript that has been accepted for publication. As a service to our customers we are providing this early version of the manuscript. The manuscript will undergo copyediting, typesetting, and review of the resulting proof before it is published in its final form. Please note that during the production process errors may be discovered which could affect the content, and all legal disclaimers that apply to the journal pertain.

Graphical Abstract:

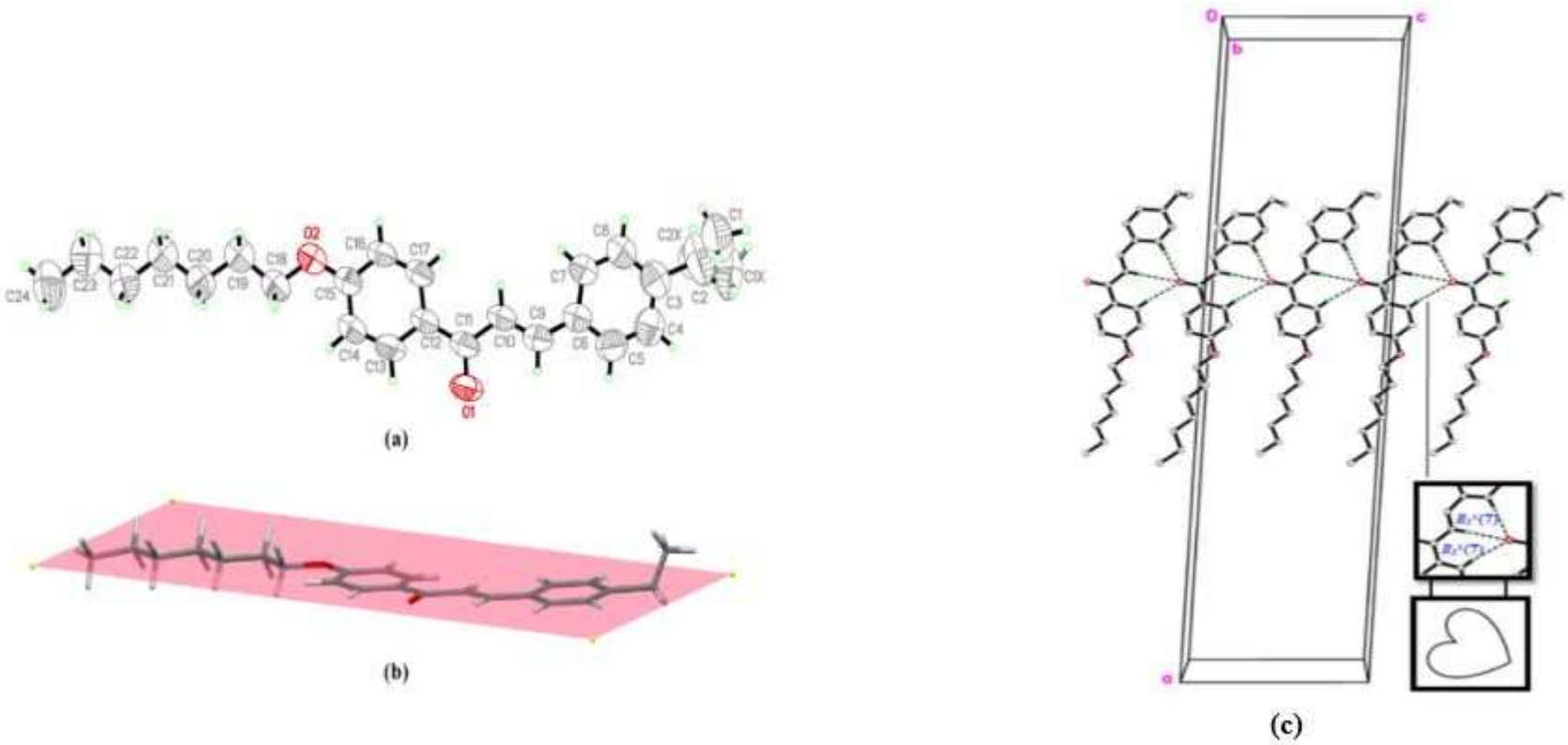

(a) The molecular structure of **4EPC** with 50% ellipsoids probability (b) The twisted ethyl group from the planarity of the compound (c) The crystal packing of **4EPC**. Dashed lines represent the intermolecular C—H···Ohydrogen bonds.

ACCEPTED MANUSCRIPT

Synthesis, spectroscopic, structural elucidation, NLO characteristic and Hirshfeld surface analysis of (*E*)-1-(4-ethylphenyl)-3-(4-(heptyloxy) phenyl)prop-2-en-1-one : A dual approach of experimental and DFT calculations

Adibah Izzati Daud[1,2], Wan M. Khairul[1,*], Elccey Augustine[1], Suhana Arshad[3], Ibrahim Abdul Razak[3]

[1]School of Fundamental Science, Universiti Malaysia Terengganu, 21030 Kuala Nerus, Terengganu, Malaysia

[2]Faculty of Engineering Technology, Universiti Malaysia Perlis (UniMAP), Level 1, Blok S2, Kampus UniCITI Alam, Sungai Chuchuh, 02100 Padang Besar, Perlis, Malaysia

[3]School of Physics, Universiti Sains Malaysia, 11800 USM Penang, Malaysia

*Corresponding author: wmkhairul@umt.edu.my

ABSTRACT

Single crystal of (*E*)-1-(4-ethylphenyl)-3-(4-(heptyloxy)phenyl)prop-2-en-1-one (**4EPC**) was grown in acetonitrile *via* slow evaporation solution technique. The molecular structure of **4EPC** was then confirmed by single crystal X-ray diffraction analysis and the crystal exhibited monoclinic with centrosymmetric space group of *C*2/*c*. The synthesised molecule of **4EPC** was fully characterized using spectroscopic techniques by Fourier-Transform infrared (FT-IR) spectroscopy, Nuclear Magnetic Resonance (^{1}H and ^{13}C NMR), thermal stability analysis *via* Thermogravimetric analysis (TGA) and electronic transitions through UV-visible analysis. In addition, the theoretical investigations on its electronic properties via UV-vis analysis of **4EPC** was calculated using time-dependent TD-DFT B3LYP/6-31G (d, p) level of theory. As predicted, the experimental results were complimentary to the theoretical findings. The Hirshfeld surface analysis contributes to the study in the aspect of the nature of intermolecular interactions as well as fingerprint plots which gave the information on the percentage contribution from each individual contact. Molecular electrostatic potential (MEP) analysis provides an initial information on the charge concentration throughout the molecule **4EPC** which designated the possible interaction site to occur. Moreover, the nonlinear optical (NLO) properties of **4EPC** was calculated to gain further understanding on the possibility of developing this compound as NLO material. Calculated NLO results found that the polarizability and 1st order hyperpolarizability of **4EPC** is -2.13 x 10^{-23} esu and 1.27 x 10^{-30} esu respectively which is greater than the value of 1st order hyperpolarizability of urea (β = 0.372 x 10^{-30} esu). The high values obtained from the calculated NLO were due to the dipole, molecular alignment and also from the non-covalent interaction within crystal of **4EPC** which can be developed further as potential organic light emitting diode application.

Keywords: alkoxy-chalcone; DFT; NLO; spectroscopic; crystal structure

1. Introduction

Chalcones are from flavonoid family that consist of two aromatic rings with different array of substitutions linked by α, β-unsaturated carbonyl moiety. These class of derivatives exhibit donor-π-donor molecular system (D-π-D) which can enhance their functionality in various fields of interest. It

possesses conjugated double bonds and a delocalized π-electron system on both aromatic rings [1-5]. Various different methods have been applied in order to synthesis chalcone derivatives, however, most reported chalcones have been synthesized by simple and inexpensive method *via* condensation as a product between aromatic aldehydes and aromatic ketones in the presence of strong base catalyst known as Claisen-Schmidt reaction [6-8]. Chalcones are bichromophoric molecules separated by ketovinylenic group (CO-CH=CH-) and π-conjugated bridges and they exhibit numerous chemical and physical properties, such as optical and fluorescence properties [9-11], electrical properties [12] and provide broad spectrum in biological activities [13-15]. Due to their excellent performances, chalcones have attracted much attention for past decades due to their potential technological application in the fields of photochemical sensors [16, 17], fluorescent probes [18], optical nonlinearities [19, 20] and as conductive organic solar cells [21, 22]. The main characteristics of functionalized chalcone derivatives are they adopt molecular flexibility, having strong donor-acceptor intermolecular interaction, rich in the delocalized π-electrons system and attaining low dielectric constant. All these unique characteristics show that chalcone derivatives hold high potential in photovoltaic devices applications.

In fact, the distinctive characteristics of low-lying π-π^* transition occurs from the aromatic ring to the alkene chain can permit the variation of the intense transition by adding suitable substituents to the aromatic ring. Electronic profile of chalcone derivatives was carried out mostly at their singlet states of π-π^* transition to determine their absorption spectra of substituted chalcones. Conjugation between substituted phenyl ring with alkene group gave a significant effect in the absorption maximum with a greater extent compared to the thiourea moiety which involves conjugation between carbonyl and aromatic ring [23]. Both systems, D-π-A and D-π-D can lower the energy level of $S_{\pi\text{-}\pi^*}$ state which is great significant in the development of molecular electronics. These promising characteristics of chalcones derivatives have attracted researchers' attention to design new classes of chalcones featuring D-π-D which should provide further understanding on structural property relationship related to non-linear optical properties. In development of new active materials in the interest of molecular electronic application such as organic light emitting diode (OLED), optical switching, photovoltaic organic solar cells and optical rectification, nonlinear optical (NLO) materials

with large and fast NLO response and their hyperpolarizabilities are crucial factors for extensive research in molecular electronic application. A large number of advanced materials have been investigated for NLO properties, in which organic materials are attractive due to their variety, high nonlinearity, ultra-fast response and the flexibility they offer to change the optical properties through structural modification. Nowadays, great attention has been given to organic NLO materials because of their first (β) and second (γ) hyperpolarizabilities and high laser damage resistance compared to inorganic materials [24, 25]. A versatile synthetic organic chemistry can be applied to prepare, modify and optimize targeted molecular structure to suit the need and requirement of molecular electronics with a desired structure to maximize their utility in advanced industrial needs. Hence, organic materials can simply be known as the "materials for future".

In the view of fundamental aspect, the structure of organic materials exhibiting NLO characteristics is based on π-bond system in which the overlapping of π-orbital increases the delocalization of electronic charge distribution that gave high mobility of the electron density which in turn exhibit enhanced optical nonlinearity related to the level of second-harmonic-generation (SHG) [26, 27] that inherently depends upon its structural attributes. Chalcone derivatives have received much consideration because of their good crystallizability and high optical nonlinearity due to its extended conjugation length. The hydrogen bonding interaction and π-π interaction are the most important factors of all intermolecular interactions due to their strength and directionality [28, 29], where the strong hydrogen bonds are widely used to build multidimensional molecular structures. The presence of strong intermolecular interactions such as hydrogen bonds can enhance level of charge transfer between molecules, owing to their electrostatic and directed nature, thereby enhancing the SHG response.

The theoretical calculations *via* quantum mechanical fluctuations techniques based on density functional theory (DFT) can support and compare with our experimental values. In recent years, our group have been involved in synthesis, characterization and computational chemistry studies of various organic molecules in vast applications [30-32]. The outcomes have proven to be highly successful in describing the structural properties and the simplest as well as the easiest methods to

understand the electronic characteristics of any molecular system of interest that having specific functionality. In fact, to identify the presence of functional groups substitution, structural behaviour, molecular interaction and absorption maxima properties, spectroscopic studies have emerged as excellent tools among materials characterisation techniques. The obtained experimental data were counterchecked by DFT calculations and in addition to this, the X-ray single crystal data sets were also compared. From DFT calculation, NLO properties of the synthesized molecule (**4EPC**) were described along with a crystal engineering of molecule to attain a centrosymmetric network.

With respect to molecular electronic development, chalcones have achieved much consideration because of their excellent NLO properties, exhibit higher power conversion energy, chemical inertness, high damage threshold and phase matching properties. Moreover, this molecular framework is also known for their excellent blue light transmittance, large NLO coefficients and short cut-off wavelength of transmission contributed mainly due to the presence of conjugated double bonds. Due to the effect from conjugation, electrons remain delocalized within the molecule and influence the performance on electron polarizability. In organic molecules, the NLO properties like molecular hyperpolarizability can be further enhanced by substituting different functional groups of both sides of chalcone which promote highly polarizable conjugated bridge. Considering both aspects of experimental and theoretical factors, the synthesis of new organic materials with enhanced NLO property (second and third order NLO) is a continuing field of research. In this direction we are reporting the synthesis and characterization of new chalcone derivatives, (*E*)-1-(4-ethylphenyl)-3-(4-(heptyloxy)phenyl)prop-2-en-1-one (**4EPC**) along with its mechanical and thermal properties.

2. Materials and methods

All chemicals, solvents and reagents used in this study namely 4-hydroxyacetophenone, 1-bromoheptane, 4-ethylbenzaldehyde, potassium carbonate, sodium hydroxide, hydrochloric acid, dimethylformamide, ethanol, hexane and ethyl acetate were purchased from well-known local and international suppliers as analytical reagents such as Merck, Across Organic, HmbG®, Sigma Aldrich and R&M Chemicals and used as received without further purifications. Reactions involved were

carried out under an ambient atmosphere without any precaution steps to omit humidity interferences during synthetic work-up.

2.1 Characterisation and instrumentation

^{1}H and ^{13}C Nuclear Magnetic Resonance (NMR) spectra were recorded in $CDCl_3$ using Bruker Avance III 400 Spectrometer in the range δ_H 0-15 ppm and δ_C 0-200 ppm accordingly with reference to the trimethylsilane (TMS) as internal standard. Fourier-Transform Infrared (FT-IR) spectra were recorded *via* Perkin Elmer 100 FT-IR spectroscopy using potassium bromide (KBr) pellets within spectral range 4000 – 450 cm^{-1}. For electronic transition analysis, UV-Visible study was performed by using Shimadzu UV-Vis in 1 cm^3 cuvette. Afterwards, thermogravimetric analysis was carried out using Perkin-Elmer TGA analyzer from 30 to 900°C at a heating rate 10° C/min under nitrogen flow consistently.

2.2 Single Crystal X-Ray Diffraction Analysis

Single crystal suitable for X-ray analysis was performed on APEXII Duo CCD area-detector using MoKα radiation (λ = 0.71073 Å). Data collection was performed using the APEX2 software [33], whereas the cell refinement and data reduction were performed using the SAINT software [33]. The crystal structure was solved by direct method using the program SHELXTL [34] and refined by full-matrix least squares technique on F^2 using anisotropic displacement parameters by SHELXTL2014 [35]. Absorption correction was applied to the final crystal data using the SADABS software [33]. All geometrical calculations were carried out using the program PLATON [36]. The molecular graphics were drawn using SHELXTL [35] and Mercury [37] programs. The non-hydrogen atoms were refined anisotropically. All the hydrogen atoms were positioned geometrically (C—H = 0.93, 0.96 or 0.97 Å) and refined using riding model $U_{iso}(H) = 1.2\ U_{eq}(C)$. The ethyl substituent group attached to one of the terminal benzene rings is disordered over two sites with refined occupancies of 0.731 (14): 0.269 (14). In the final refinement, one outlier (2 0 0) was omitted. A summary of crystal data and relevant refinement parameters of the title compound is given in Table 1.

ACCEPTED MANUSCRIPT

Table 1 Crystallographic refinement data.

Refinement Parameters	
CCDC deposition numbers	CCDC 1867813
Molecular formula	$C_{24}H_{30}O_2$
Molecular weight	350.48
Crystal system	Monoclinic
Space group	*C2/c*
a (Å)	46.746 (7)
B (Å)	8.3426 (12)
C (Å)	10.8945 (15)
α (°)	90.00
β (°)	92.993 (5)
γ (°)	90.00
V (Å^3)	4242.9 (10)
Z	8
D_{calc} (Mg m^{-3})	1.097
Crystal Dimensions (mm)	0.46 x 0.45 x 0.25
μ (mm^{-1})	0.07
Radiation λ (Å)	0.71073
F(000)	1520
T_{min}/T_{max}	0.8561/ 0.9534
Reflections measured	55021
Ranges/indices (*h*, *k*, *l*)	$h = -60 \rightarrow 60$
	$k = -10 \rightarrow 10$
	$l = -14 \rightarrow 14$
θ limit (°)	1.8 - 27.7
Unique reflections	4917
Observed reflections ($I > 2\sigma(I)$)	1846
Parameters/Restraint	258/1
R_1 [a], wR_2 [b] [$I \geq 2\sigma(I)$]	0.060/0.226
Goodness of fit [c] on F^2	0.99
R_{int}	0.075
Largest diff. peak and hole, e/Å^{-3}	0.15 and − 0.10

$w = 1/[\sigma^2(F_o^2) + (0.0943P)^2 + 0.8318P]$, where $P = (F_o^2 + 2F_c^2)/3$; [a] $R = \Sigma||F_o| - |F_c||/\Sigma|F_o|$, [b] $wR = \{w\Sigma(|F_o| - |F_c|)^2/\Sigma w|F_o|^2\}\}^{1/2}$, [c] $GOF = \{\Sigma w(|F_o| - |F_c|)^2/(n-p)\}^{1/2}$, where *n* is the number of reflections and *p* the total number of parameters refined.

2.3 Theoretical calculations: Density functional theory (DFT)

All the involved theoretical calculations were executed by Gaussian 09 program package [38] featuring density functional theory (DFT). The initials geometry for **4EPC** was retrieved from the crystal structure. Optimization of **4EPC** was carried out without using symmetry restrictions at the theoretical level of DFT B3LYP/6-31G (d, p) basic set known to be as a practical strategy to compute

the structure of **4EPC**. FMOs and MEP properties were also executed at B3LYP/6-31G (d, p) level of theory. Theoretical electronic transition for **4EPC** was computed employing time-dependent density functional theory (TD-DFT) with B3LYP level and 6-31G (d, p) basis set, while the input file and data interpretation were organized and utilized *via* GaussView 5.0 [39].

3. Experimental work

3.1 Synthesis of 4-heptyloxyacetophenone

Reaction work-up details with respect to the synthesis of precursor 4-heptyloxyacetophenone followed as stated in the previous literature [40]. 4-hydroxyacetophenone (0.14 g, 1 mmol), 1-bromoheptane (0.18 g, 1 mmol) and potassium carbonate (0.40 g, 3 mmol) were charged into 2-neck round bottom flask with 65 mL of dimethylformamide (DMF). The reaction mixture was put at reflux with continuous stirring for 24 hours. Once the reaction was adjudged completion using Thin Layer Chromatography (TLC) hexane: ethylacetate: 3:2, the reaction mixture was cooled to room temperature, then poured over to 50 mL water and extracted with hexane (50 mL x 2). The organic fractions collected was separated and washed with 1M aqueous NaOH (25 mL) and then with aqueous 1M HCl (25 mL). Organic layer obtained was dried over Na_2SO_4 and continually dried under reduced pressure to yield 4-heptyloxyacetophenone. Scheme 1 illustrates the synthetic pathway to synthesis 4-hydroxyacetophenone.

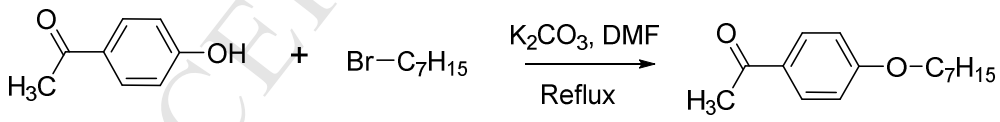

Scheme 1. Synthesis of 4-hydroxyacetophenone.

*3.2 Synthesis of (E)-1-(4-ethylphenyl)-3-(4-(heptyloxy) phenyl) prop-2-en-1-one (**4EPC**)*

4EPC was synthesised *via* Claisen-Schmidt condensation reaction between substituted ketone and aldehyde derivatives. The analytical grade starting material of *p*-ethylbenzaldehyde (0.13 g, 1 mmol) and the synthesised 4-hydroxyacetophenone (**1**) (0.23 g, 1 mmol) were dissolved in ethanol (40 mL) in the presence of catalytic amount of 15% NaOH solution (approximately 15 mL) was added

drop-wise to the solution with vigorous stirring and put at reflux for *ca*. 3-4 hours. Once the reaction was adjudged completion *via* Thin Layer Chromatography (TLC) hexane: ethylacetate: 3:2, the reaction mixture was cooled to room temperature and then poured into beaker containing some ice cubes. The resulting precipitate were then filtered, washed with distilled water and dried over silica gel. The obtained crude product was subjected to recrystallisation from methanol to obtain the corresponding alkoxy-chalcone derivative (**4EPC**) as in Scheme 2.

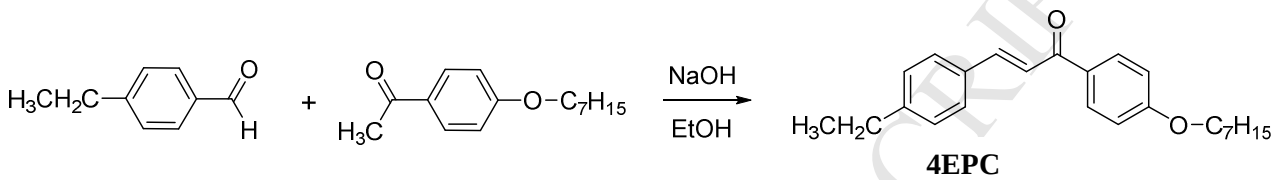

Scheme 2. Synthesis of **4EPC**.

4. Results and discussion

4.1 Spectroscopic studies

4.1.1 NMR analysis

The synthesised molecule (**4EPC**) was obtained *via* simple Claisen-Schmidt method in good yield. To elucidate the synthesis of our targeted molecule, **4EPC** was characterized *via* following spectroscopic techniques. ^{1}H and ^{13}C NMR spectra were recorded operating at 400 MHz and 100.6 MHz for ^{1}H and ^{13}C respectively using standard parameters in $CDCl_3$ solvent and trimethylsilane (TMS) was used as an internal standard. Both ^{1}H and ^{13}C NMR spectra of **4EPC** are shown in Supplementary material 1. ^{1}H NMR spectrum of **4EPC** revealed triplet resonances at shielding position of δ_H 0.828 ppm corresponded to the methyl (aliphatic) proton. Whilst, for methyl substitution at aromatic position, the triplet resonances can be observed at δ_H 1.187 ppm. Multiplet overlapping resonances at region δ_H 1.220 – 1.762 ppm were attributed to the CH_2 (aliphatic) group. However, CH_2O was positioned at the deshielded region at δ_H 3.965 ppm due to the electronegative effect from oxygen atom nearby. Additionally, there were aromatic phenyls protons appeared at δ_H 6.884 – 7.996 ppm corresponding to total of eight protons. The two doublets at δ_H 7.464 ppm and δ_H 7.702 ppm with

characteristic coupling constants (*J*) of 15.6 Hz for both doublets are corresponded to α, β-unsaturated protons (CH=CH) of aliphatic groups [41, 42]. The higher value of coupling constant proved the existence of *E*-geometry of double bond in chalcones and also confirmed the purity of the synthesized **4EPC**. For the ^{13}C NMR, nine signals within shielded range δ_C 13.1 – 67.3 ppm represents alkyl carbons. The aromatic phenyls carbons appeared at δ_C 127.5 – 161.9 ppm. Two consecutive moderate signals at δ_C 113.2 ppm and δ_C 119.9 ppm are due to the presence of α, β-unsaturated carbons. The peak resonated at δ_C 187.8 ppm was attributed to the presence of carbonyl (C=O) carbon atom.

4.1.2 Vibrational analysis

The FT-IR spectrum of **4EPC** was recorded using Perkin Elmer 100 FTIR spectrophotometer within the spectral range 4000-450 cm^{-1}. The experimental and simulated FTIR spectrum using DFT(B3LYP) method using 6–31G (d, p) functional are shown in Supplementary material 2. All the experimental and theoretical vibrational frequencies for the synthesized compound, along with corresponding vibrational assignments are given in Table 2. From experimental data, it showed five absorption bands of interest represents the bending of CH_3, CH (alkane), C=C, C=O and CH aromatic. The sharp absorption band at 1650 cm^{-1} is due to the carbonyl (C=O) stretching of α, β-unsaturated carbonyl group while the DFT calculation gives this mode at 1642 cm^{-1}. Absorption of C=O was observed at lower wavenumber due to the effect from delocalization of π-electrons between α and β carbons which decreases the C=O order and thus, increasing the bond order between the carbonyl carbon and α carbon atom. Additionally, another characteristic band shown by chalcone was C=C stretching vibration between 1602 cm^{-1} and 1464 cm^{-1} in the IR spectrum and at 1588 and 1623 cm^{-1} theoretically, at which the wavenumbers were varies depending on the substituents group attached to the chalcones molecular framework. Moreover, the medium intensity bands at around 2869 cm^{-1} – 2938 cm^{-1} are attributed to aliphatic C-H stretching vibrations while the DFT calculated vibration for C-H were observed in the range 3119 – 3174 cm^{-1}.Whilst two distinctive peaks at 1464 cm^{-1} and 1396 cm^{-1} in the IR spectrum and 1324 – 1394 cm^{-1} theoretically due to the presence of CH_3 (bending). Weak intensity bands at 3082 cm^{-1} (experimentally) and theoretically at 3058 – 3069 cm^{-1} was assigned to C-H (aromatic).

ACCEPTED MANUSCRIPT

Table 2 Experimental and theoretical vibrational frequencies of the compound and their respective assignments.

	Theoretical IR (B3LYP/6-31G (d, p))			
Experimental IR (cm^{-1})	Freq (Scaled), cm^{-1}	Intensity	Unscaled freq, cm^{-1}	Vibrational assingments
	3174	15.75	3229	υCH
	3168	22.88	3222	υCH
	3160	1.01	3214	υCH
	3156	3.07	3211	υCH
	3146	14.78	3200	υCH
	3142	1.43	3196	υCH
	3137	20.99	3191	υCH
	3119	15.46	3173	υCH
	3118	17.19	3172	υCH
3082	3113	1.70	3167	υCH
	3069	30.58	3122	υCH
	3065	51.65	3118	υCH
	3058	42.38	3111	υCH
	3053	66.93	3105	υCH
	3041	73.60	3094	υCH
	3027	8.83	3080	υCH
	3019	58.19	3071	υCH
	3004	0.03	3056	υCH
	2994	41.68	3045	υCH
	2993	23.57	3045	υCH
	2992	38.24	3044	υCH
	2990	38.38	3042	υCH
	2990	0.11	3041	υCH
	2986	43.89	3037	υCH
	2983	0.17	3035	υCH
	2975	80.21	3027	υCH
	2968	12.50	3020	υCH
2938	2962	3.74	3013	υCH
	2959	0.62	3010	υCH
2869	2953	23.09	3004	υCH
	1707	126.29	1737	υC=O
1650	1642	146.99	1671	υC=O
	1632	573.23	1660	υC=O
	1623	139.94	1651	υC=O
1602	1588	0.34	1616	υCC
	1584	34.21	1612	υCC
	1530	9.76	1557	υCC

ACCEPTED MANUSCRIPT

	1528	52.54	1554	υCC
	1508	49.24	1534	υCC
	1502	6.12	1527	υCC
	1496	1.72	1522	υCC
	1495	5.78	1521	υCC
	1487	5.56	1513	υOC
	1487	0.46	1512	υCC
	1485	7.36	1511	υCC
1464	1480	0.36	1506	υCC
	1475	2.27	1501	υCC
	1475	0.04	1501	υCC
	1474	0.36	1500	υOC
	1438	21.57	1463	υCC
	1434	15.92	1459	υCC
	1416	37.31	1440	υCC
	1403	0.86	1427	υCC
1396	1398	2.71	1422	υCC
	1394	1.49	1418	υCC
	1384	1.08	1408	*b*CCC
	1355	310.23	1378	*b*CCC
	1345	5.29	1368	*b*HCC
	1342	1.26	1365	*b*HCC
	1338	16.30	1361	*b*HCC
	1334	76.02	1358	*b*HCH
	1330	13.72	1353	*b*HCH
	1324	0.18	1346	*b*HCH
	1319	0.30	1342	*b*HCC
	1305	0.03	1328	*b*HCC
	1305	60.96	1327	*b*HCC
	1302	7.15	1325	*b*HCH
	1297	0.06	1320	*b*HCC
	1289	102.65	1311	*b*HCC
	1280	406.12	1303	*b*HCC
	1255	0.23	1277	*b*HCC
	1255	1.19	1277	*b*HCC
	1231	0.92	1253	*b*HCO
	1225	297.69	1246	*b*HCH
	1219	1.60	1240	*b*HCC
	1210	21.71	1231	*b*HCH
	1209	0.64	1230	*b*HCC
	1189	2.72	1210	*b*HCH
	1176	1.06	1197	*b*HCC
	1174	450.87	1194	*b*HCC
	1130	11.54	1150	*b*HCC
	1128	15.49	1148	*b*HCH
	1123	4.61	1143	*b*HCC

ACCEPTED MANUSCRIPT

1068	2.69	1087	*b*HCH
1065	21.13	1084	*b*HCH
1054	9.40	1072	*b*HCH
1053	7.32	1071	*b*HCH
1047	60.02	1065	*b*OCC
1041	1.58	1059	*b*CCC
1033	164.17	1051	*b*CCC
1018	19.29	1036	*b*CCC
1017	1.35	1035	*b*CCC
1014	48.10	1031	*b*CCC
1013	0.46	1031	*b*CCC
1004	25.06	1021	*b*CCC
985	2.55	1002	*b*CCC
976	0.27	992	*b*OCC
957	5.04	974	*b*CCC
952	0.24	968	*b*CCC
948	0.27	965	*b*CCC
936	1.01	952	*b*CCC
926	0.01	942	*b*CCO
893	2.52	908	*b*COC
887	0.60	902	*b*CCC
869	0.36	884	*b*CCC
846	6.04	861	*b*CCC
837	0.91	852	*b*CCC
836	13.63	850	*b*CCC
831	0.40	845	*b*CCC
823	73.10	837	τHCCC
812	0.37	826	τHCCC
802	5.70	815	τHCCC
781	0.77	794	τHCCC
774	1.68	788	τHCCC
755	8.29	768	τHCCC
737	0.21	749	τHCCC
730	4.15	742	τHCCC
725	4.64	737	τHCCC
718	3.65	731	τHCCC
674	3.26	686	τHCCC
645	2.31	656	τHCCC
637	31.65	648	τHCCC
633	43.92	644	τHCCC
554	22.31	563	τHCCC
537	2.56	546	τHCOC
518	7.22	527	τHCOC
509	1.54	518	τHCCC
492	13.34	500	τHCCC
465	0.81	473	τHCCC

446	4.86	453	τHCCC
416	0.02	423	τHCCC
410	0.34	417	τHCCC
394	1.01	401	τHCCC
376	1.43	383	τHCCC
364	0.96	370	τHCCC
340	0.10	346	τHCCC
302	0.19	308	τHCCC
289	5.62	294	τHCCC
263	0.74	267	τHCCC
242	0.01	246	τCCCC
238	0.02	242	τCCCC
216	0.07	220	τCCCC
213	1.37	217	τCCCC
171	2.16	174	τCCCC
162	0.82	165	τCCCC
158	0.05	161	τCCCC
146	1.67	149	τCCCC
136	0.39	139	τCCCC
130	0.62	132	τCCCC
116	0.36	118	τCCCC
106	0.01	108	τCCOC
96	0.44	98	τCOCC
84	1.49	85	τCCCO
61	0.22	62	τCCCC
51	0.19	52	τCCCC
47	0.02	48	τCCCC
43	0.11	44	τCCCC
32	0.03	33	τCCCC
26	0.47	26	*w*OCCC
20	0.09	20	*w*OCCC
14	0.04	14	*w*CCCC
11	0.05	11	*w*CCCC

v:stretching; b:in plane bending; w:out-of-plane bending; τ: torsion.

4.2 Molecular and Crystal Structures Analysis

The molecular structure of **4EPC** (Fig. 1. (a)) crystallizes in monoclinic crystal system with *C2/c* space group where the unit cell parameters are a = 46.746 (7) Å, b = 8.3426 (12) Å, c = 10.8945 (15) Å, β = 92.993 (5)°, $\alpha = \gamma$ = 90° and Z=8. The-para substituted ethyl group (C1 and C2) on the terminal phenyl ring is disordered over two positions with refined site occupancies ratio of 0.731 (14): 0.269 (14). The bond lengths and angles are within the normal ranges and comparable with the

previously reported structures of chalcone [43-45]. Table 3 lists the bond lengths and angles of the optimized structure in comparison to the experimental values. The molecular structure of **4EPC** adopts *s-cis* configuration with respect to the C11=O1 and C9=C10 double bond distances of 1.227 (2) Å and 1.319 (3) Å, respectively. The ethyl substituent group is found to be twisted (Fig. 1. (b)) from the essentially planar molecular structure [maximum deviation of 0.143 (4) Å at atom C24] with the C1—C2—C3—C4 torsion angles being −106.5 (16)°. The corresponding torsion angle value for minor part (C1X—C2X—C3—C4) is −30 (3)°. These torsion angle values showing that the major and minor disordered ethyl groups are oriented in –*anti*-clinal and –*syn*-clinal conformations, respectively. Furthermore, the planarity of the **4EPC** is shown by the dihedral angles formed between the enone moiety (O1/C9-C11; maximum deviation of 0.001(3) Å) with the terminal benzene ring (C3-C8) and (heptyloxy)benzene moiety (O2/C12-C24) which are 3.77 (18)° and 0.73 (15)°, respectively.

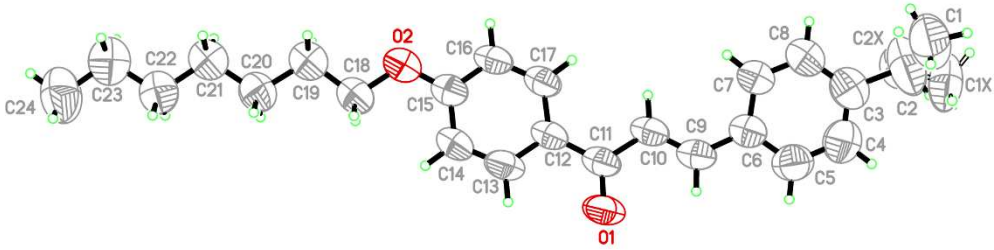

(a)

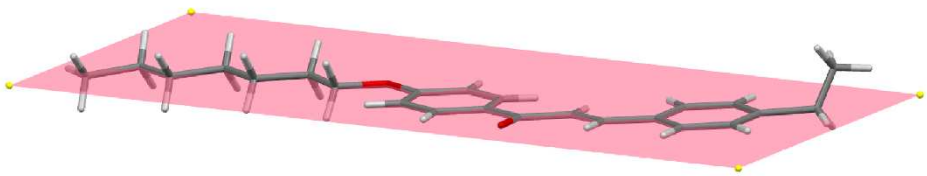

(b)

Fig. 1. (a) The molecular structure of **4EPC** with 50% ellipsoids probability with atomic numbering scheme. All disordered components are shown (b) The twisted ethyl group from the planarity of the compound where the minor disordered part has been omitted for clarity.

Table 3 Selected bond lengths and angles of the title compound.

Atoms	Geometric parameters (Å)	
	Experimental	DFT (B3LYP/6-31G (d,p)
Bond Lengths (Å)		
O1—C11	1.227 (2)	1.232
O2—C15	1.356 (3)	1.359
O2—C18	1.423 (3)	1.430
C6—C9	1.443 (3)	1.461

ACCEPTED MANUSCRIPT

C9—C10	1.319 (3)	1.348
C10—C11	1.458 (3)	1.485
C11—C12	1.476 (3)	1.496
Bond Angles (°)		
C1—C2—C3	116.0 (18)	112.8
C10—C9—C6	128.6 (2)	128.2
C9—C10—C11	121.1 (2)	119.7
C10—C11—C12	120.7 (2)	119.3
O1—C11—C10	119.7 (2)	120.7
C15—O2—C18	118.44 (19)	119.1
Torsion Angles (°)		
C1—C2—C3—C4	−106.5 (16)	-91.4
C5—C6—C9—C10	−178.6 (2)	179.9
C6—C9—C10—C11	−178.3 (2)	179.6
C9—C10—C11—O1	−0.2 (4)	-2.5
C9—C10—C11—C12	178.9 (2)	177.9
O1—C11—C12—C13	−0.6 (4)	-5.4
C18—O2—C15—C16	179.4 (2)	-179.7
O2—C18—C19—C20	178.03 (19)	-179.9
C18—C19—C20—C21	−178.9 (2)	179.9
C19—C20—C21—C22	175.2 (2)	-179.9
C20—C21—C22—C23	179.9 (2)	179.9
C21—C22—C23—C24	178.4 (3)	-179.9

The crystal packing of **4EPC** is shown in Fig. 2. The intermolecular C7—H7A···O1, C10—H10A···O1 and C17—H17A···O1 hydrogen bonds (Table 4, symmetry code: *x*, −*y*+1, *z*−1/2) link the molecules into a heart-shape character by the formation of two $R_2^1(7)$ graph-set motifs [46]. These heart-shape motifs are further connected into one-dimensional chain along the *c*-axis. The strong intermolecular C—H···O hydrogen bonds (D—H···A angle: 170-176°) shows that the oxygen atom (O1) of the carbonyl group has become the most reactive sites for a nucleophilic attack of the hydrogen atoms from the chalcone ethylenic bridge and phenyl rings. Furthermore, the infinite one-dimensional chains are also observed to cross-link with each other and stack along the *b*-axis.

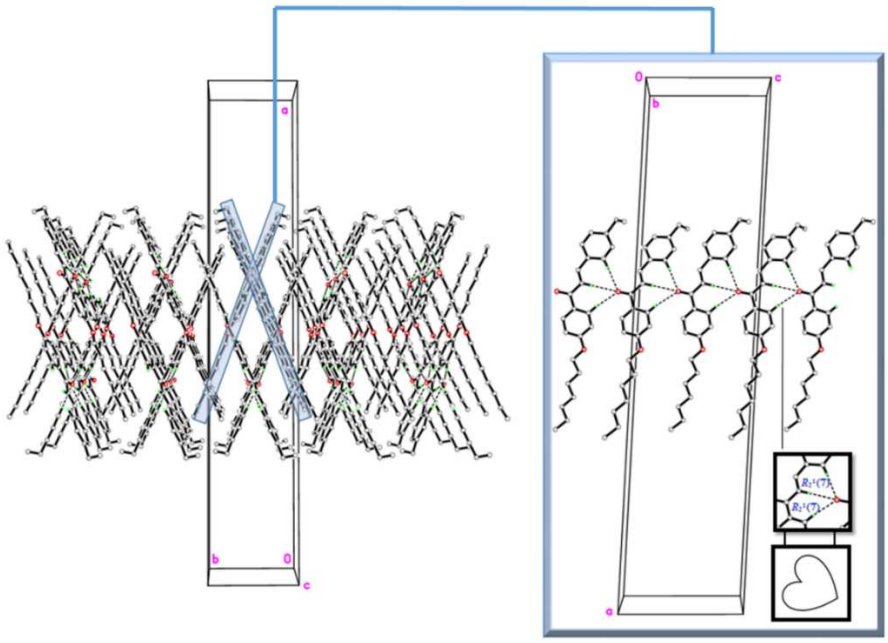

Fig. 2. The crystal packing of **4EPC**. Dashed lines represent the intermolecular C—H···Ohydrogen bonds. Only major disordered components are shown.

Table 4 Hydrogen bond geometry of the compound.

Bond	**Bond length, (Å)**			**Angle**
D—H···A	**D—H**	**H···A**	**D···A**	**D—H···A, (°)**
C7—H7A···O1$^{(i)}$	0.93	2.50	3.427 (3)	176
C10—H10A···O1$^{(i)}$	0.93	2.47	3.394 (3)	171
C17—H17A···O1$^{(i)}$	0.93	2.49	3.407 (3)	170

Symmetry codes: (i) x, $-y+1$, $z-1/2$.

4.3 Thermal analysis

The thermal stability of the prepared **4EPC** was evaluated using thermogravimetric analysis (TGA) under nitrogen atmosphere and the obtained data are presented in Table 5, whereas Fig. 3 depicts TGA and DTG thermogram of **4EPC**.

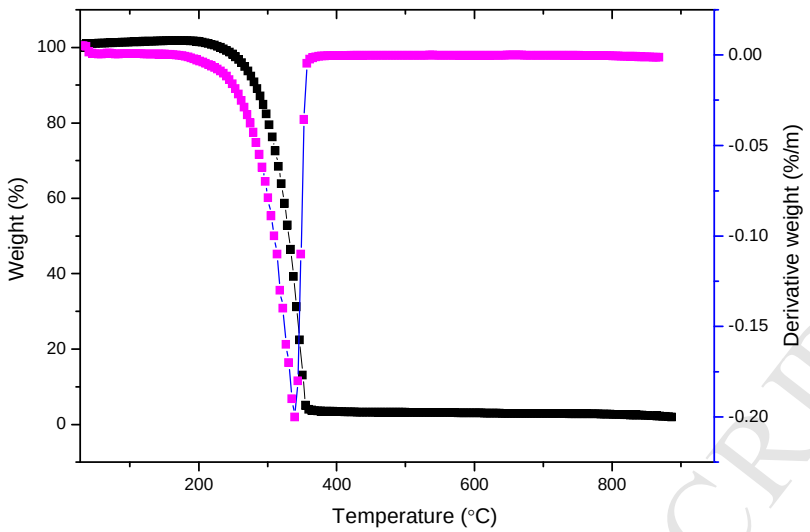

Fig. 3. TGA with DTG thermogram of **4EPC**.

The thermal behavior of **4EPC** was recorded from ambient temperature up to 900 °C in nitrogen flow and did not show any weight loss up to 276 °C, indicated that crystal water molecules and coordinated water molecules are not present in compound **4EPC**. The results obtained from TGA/DTG curves reveals that compound **4EPC** started to degrade in single step at onset temperature (T_d) 276 °C, with maximum degradation occurred at 346 °C. The single decomposition stage occurred in the temperature range of 276 – 355 °C with a mass loss of 95.2% consistent with the evaluation of (*E*)-1-(4-ethylphenyl)-3-(4-(heptyloxy) phenyl) prop-2-en-1-one (loss of weight calculated 95.7%). The final residue mass loss was about 4.8% which correspond to the char residue of CH_3. Compound **4EPC** decomposes at high temperature due to the introduction of long alkoxy chain in the molecular framework. This high thermal stability of **4EPC** probably arises because in its crystal packing, the long chain is further stabilized by π-stacking between adjacent aromatic, carbonyl and C=C alkene. In fact, the high thermal stability of **4EPC** agrees with the nearly planar structure of **4EPC**, favours in this way the donor→donor interactions, through the intermolecular interactions of C—H···O hydrogen bonds. Generally, the thermal behaviour obtained are supported with the previously reported related compounds [47, 48] in term of their stability and stage of degradation.

ACCEPTED MANUSCRIPT

Table 5 Thermal stability analysis of **4EPC**.

Compound	Onset temperature, T_d (°C)	Weight loss (%)	Expected moieties decomposition	Final residue (%)
4EPC	276	276 – 355 °C (95.2%); [calc: 95.7%]	(E)-1-(4-ethylphenyl)-3-(4-(heptyloxy) phenyl) prop-2-en-1-one	4.8

4.4 UV-visible analysis

Electronic absorption spectrum of **4EPC** was recorded in the 200 – 600 nm range in dichloromethane (DCM) solvent (c = 1 x 10^{-5} M). The value of maximum wavelength (λ_{max}) of absorption of molecule **4EPC** was observed at 327 nm while the cut-off wavelength (λ_{edge}) is at 368 nm represent the intraligand charge transfer transitions of an electron from bonding to anti-bonding ($\pi \rightarrow \pi^*$) which were attributed by aromatics nuclei and alkene C=C chromophores. Whilst, the absorption minimum arised from electronic transition of non-bonding to anti-bonding ($n \rightarrow \pi^*$) which was contributed from moieties C=O and C-O chromophores. The experimental and TD-DFT UV-vis of **4EPC** are shown in Fig. 4. Thus, the optical energy band gap for molecule **4EPC** is 3.37 eV according to the formula of $\Delta E_{gap} = hc/\lambda_{edge}$. TD-DFT is currently developed to determine the dynamic and static features of the compounds in their excited states, allowing for the correlation between computational output and experimental data based on the TD-DFT B3LYP/6-31G (d, p) level of theory. The predictions were carried out in solvation model, in which IEF-PCM formalism was considered. The calculated wavelength (λ), oscillator strength (f_o), excitation energies (eV) and spectral assignments with major contributors are shown in Table 6. Calculated UV-vis spectrum of **4EPC** exhibited two intense allowed transition at λ_{max} = 347 nm, f_o = 1.1197 and λ = 313 nm, f_o = 0.1213 which are corresponded to the experimental λ_{max} value of 327 nm. In fact, the theoretical transition peaks for **4EPC** in DCM are red-shifted compared with the experimental data in which, the assigned bands were attributed with HOMO→LUMO ($n \rightarrow \pi^*$) and HOMO-1→LUMO ($\pi \rightarrow \pi^*$) transitions. For a better description of the electronic properties, the character of the orbitals involved in the main electronic transitions of compound **4EPC** are illustrated in Figure 5. The HOMO is attributed to a π bonding system localized over phenyl and C=C moieties and a p-type orbital strongly located on the oxygen atom. The HOMO-1 corresponds to a π bonding system spread over phenyl, C=C and

carbonyl (C=O) moieties and a p-type orbital strongly located at the oxygen atom similar as described for HOMO. In LUMO, electrons were spread to the entire molecules except for alkoxy chain.

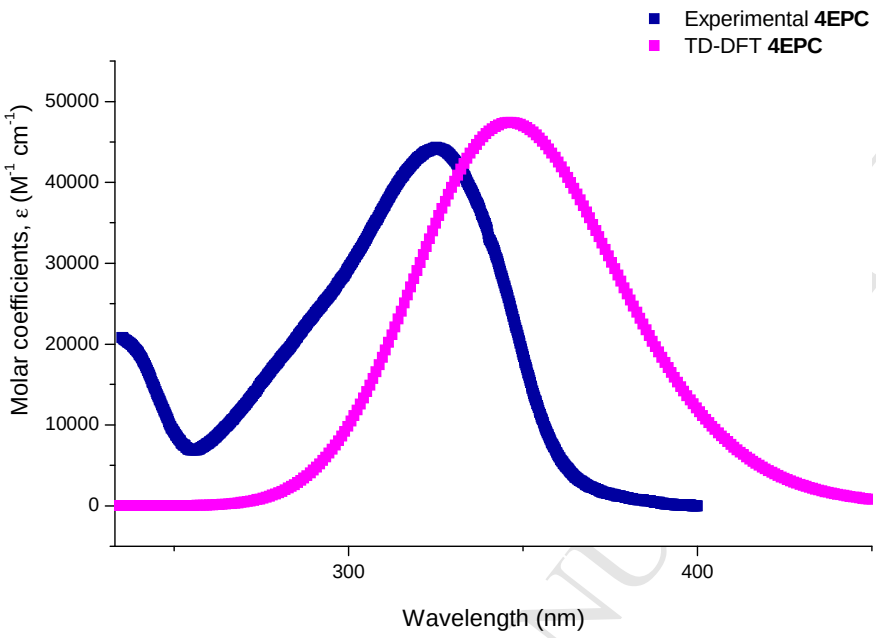

Fig. 4. The experimental and TD-DFT UV-vis for synthesized molecule **4EPC**.

Table 6 The excitation energy, oscillator strength, calculated and experimental wavelength (nm) and major contributions of electronic transitions from ground state (S_0) to excited state (S_n).

Molecule	Wavelength (nm)		Oscillator strength (f_o)	Electronic transition	Excitation energies (ΔE, eV)	Assignments, major contributors (%)
	Experimental	Calculated				
4EPC	327	347	1.1197	$S_0 \rightarrow S_1$	3.56	HOMO→LUMO (97%)
		313	0.1213	$S_0 \rightarrow S_2$	3.95	HOMO-1→LUMO (96%)

4.5 Frontier molecular orbitals (FMOs) analysis

The analysis of frontier molecular orbitals (FMOs) plays an important role to understand the chemical stability of a molecule. The FMOs of the synthesised **4EPC** was computed *via* TD-DFT approach with B3LYP/6-31G (d, p) and are illustrated in Fig. 5. The HOMO-LUMO energy gaps determine the chemical reactivity, chemical hardness and softness as well as the polarizability of the synthesised molecule. In the case of **4EPC**, the HOMO-LUMO energy gap is relatively small, *i.e.* 4.02 eV, indicating molecule **4EPC** is soft which can exhibit good polarizability and nonlinear optical

(NLO) properties. FMOs results revealed that the electron distribution in HOMO were spread mostly on ethylenic bridge and aromatic rings with donor-donor substitution. However, in LUMO level, the charge density is confined over the entire molecules (including ethylenic bridge, aromatic rings and carbonyl functional group) except for alkoxy chain substitution. Moreover, for HOMO-1 and LUMO both also lie almost over the whole molecule except at alkoxy chain. For **4EPC**, there are two electronic excitation energies were involved, i.e. the transition of electrons from the ground state (S_0) to the excited state (S_n), and the percentage of major contributions which the findings are tabulated in Table 5. The first excitation energy involved ($S_0 \rightarrow S_1$) is 3.56 eV which are in close argument with the experimental energy band gap 3.37 eV with 97% of the involved electronic transition is from ground state to the first excited state are HOMO→LUMO transition and 96% of the transitions are HOMO-1→LUMO involved in the second excitations ($S_0 \rightarrow S_2$) with the energy separation of 3.95 eV. The energy separation between the HOMO and LUMO as well as their atomic orbitals compositions known to have synergetic effect within the molecule, which subsequently affects the NLO properties of each compound. From the obtained FMOs and electronic analysis suggest that the grown crystal of **4ECP** can be the promising and potential candidate for optoelectronic devices.

Furthermore, the global chemical reactivity descriptors (GCRD) are another vital technique to understand the chemical properties of a molecule such as chemical hardness (η), chemical potential (μ), chemical softness (*S*), electronegativity (χ) and electrophilic index (u). The formula (Eq. 1 to Eq. 5) to obtain GCRD is derived from HOMO-LUMO energies, taking the HOMO energy as ionization potential (*I*) and LUMO as electron affinity (*A*) and the data are tabulated in Table 7.

Chemical hardness (η) = $[(E_{LUMO} - E_{HOMO})/2]$ Eq. 1

Chemical softness (*S*) = $[1/2\eta]$ Eq. 2

Chemical potential (μ) = $[(E_{HOMO} + E_{LUMO})/2]$ Eq. 3

Electronegativity (χ) = $[(I + A)/2]$ Eq. 4

Electrophilic index (u) = $[\mu^2/2\eta]$ Eq. 5

From the calculation, it was found that **4EPC** is kinetically stable with the hardness value of 2.01 eV, chemical potential of -4.09 eV, chemical softness of 0.25 $e^{-1}V^{-1}$ electronegativity of 4.09 eV and the electrophilic index of 4.16 eV suggest that **4EPC** possess excellent chemical strength and stability.

Table 7 Molecular orbitals energies of HOMO and LUMO (eV) and the global chemical reactivity descriptors (GCRD).

Molecule	E_{HOMO}	E_{LUMO}	ΔE (eV)	η (eV)	μ (eV)	S ($e^{-1}V^{-1}$)	χ (eV)	u (eV)
4EPC	-6.1019	-2.0762	-4.02	2.01	-4.09	0.25	4.09	4.16

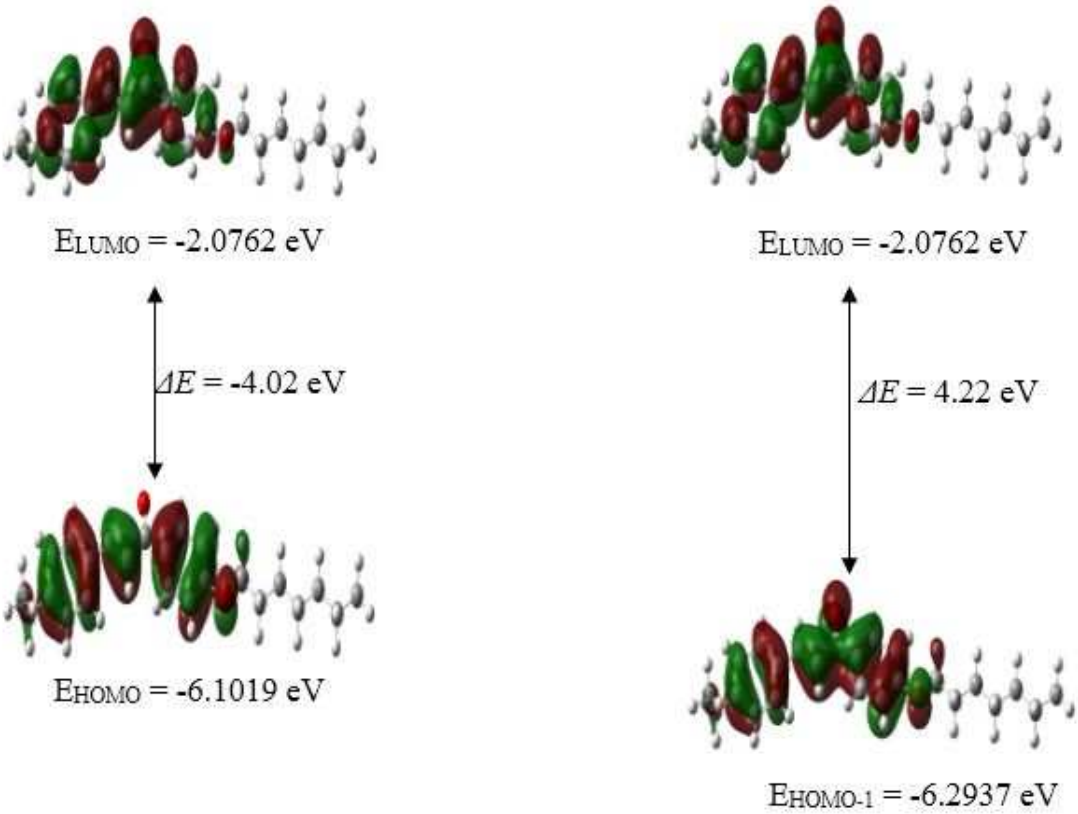

Fig. 5. Molecular orbitals of title molecule **4EPC.**

4.6 Hirshfeld surface analysis

The intermolecular interaction, packing mode and molecular shape of the crystal structure of **4EPC** was studied using Hirshfeld surface analysis (HSA). The HSA is mapped with d_{norm} (Fig. 6) and 2D fingerprint analysis plot for the crystal **4EPC** was generated by Crystal Explorer 3.1 program using crystallographic output file (.cif) obtained from single crystal X-ray diffraction. The 2D fingerprint plot analysis of **4EPC** was illustrated in Fig. 7, consists of distribution graph of d_e *vs* d_i where d_e and d_i are the distance from a point on the Hirshfeld surface to the nearest nucleus inside the surface and outside the surface, respectively. The H-H and C-H interactions are the major intermolecular interactions in the crystal structure of **4EPC** (65.3% and 13.5%). Single sharp spike at the bottom area was observed at the bottom left of 2D fingerprint plot, depicts the O-H interaction (5.2%) in the **4EPC** crystal structure which corresponded to the weak intermolecular C-H/O hydrogen bond represent at the circular depressions (deep red) visible on the Hirshfeld surface. Moderate spike at the top right region indicates H-C interaction (11%), whilst, the single sharp spike at top region indicates H-O interaction (4.4%). Strong interaction is determined by the more space occupied compared to the weak interaction with less space occupied in the fingerprint plot. The combination of d_e and d_i in the form of a 2D fingerprint plot give an information of intermolecular contact in the crystal.

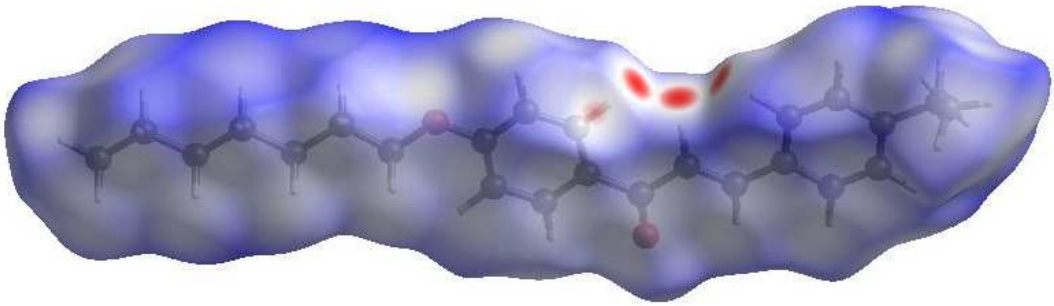

Fig. 6. The Hirshfeld surface of **4EPC** mapped with d_{norm}.

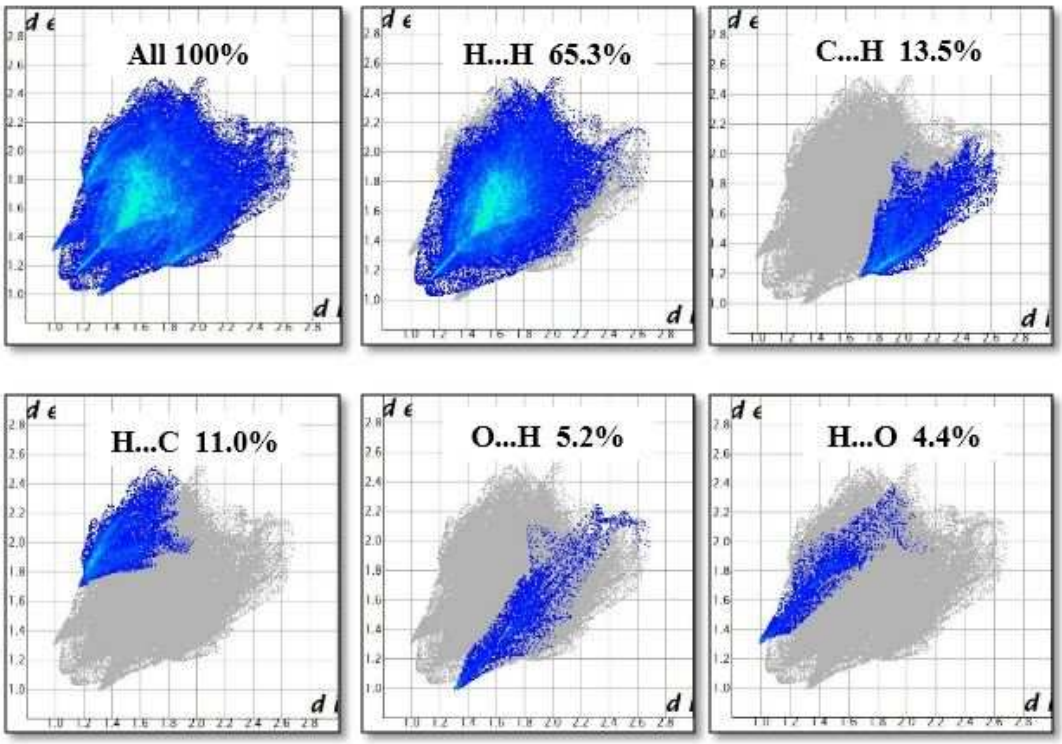

Fig. 7. The 2D fingerprint plot of crystal **4EPC** and the percentage of contribution to the total Hirshfeld area.

4.7 Molecular electrostatic potential (MEP) analysis

The molecular electrostatic potential (MEP) analysis is one of the important tools to determine the possible interaction site within **4EPC** where the reactivity of **4EPC** can be determined by predicting the nucleophilic and electrophilic sites of the molecule. The computed MEP using DFT B3LYP/6-31 G (d, p) is as shown in Fig. 8 in which the mapped MEP surface gives us information on the charge distribution region of a molecule. The distribution of charges governs the molecule interaction and the nature of the chemical bond. The nucleophilic region of the molecule is described by the positive area of MEP surface while the electrophilic site of the molecule is associated with the negative region of MEP surface. For **4EPC**, the negative charges are more concentrated on the oxygen atom of carbonyl (C=O) with the colour code of the map is in the range between -5.825 x 10^{-2} a.u.

(deepest red) towards 5.825 x 10^{-5} a.u. (deepest blue) in the map. This revealed that the oxygen atom from C=O is the most reactive site to interact favourably with nucleophile.

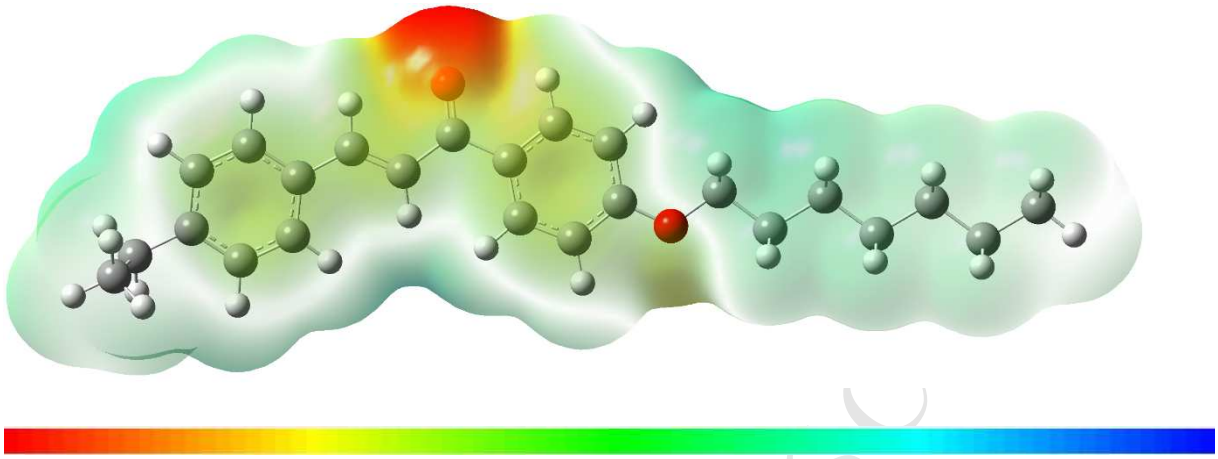

Fig. 8. MEP surface of molecule **4EPC**.

4.8 Nonlinear optical (NLO) properties: DFT calculation

Density functional theory (DFT) calculation was used to examine nonlinear optical (NLO) properties for **4EPC** in term of dipole moment (μ), polarizability (α) and 1st hyperpolarizability (β) indexes. The polarizability and hyperpolarizability components are the derivatives of molecular energy with respect to the strength of applied electric field. The static dipole moment, polarizability and 1st hyperpolarizability were calculated *via* DFT B3LYP/6-31G (d, p) and were calculated using the following equations and the related parameters are tabulated in Table 8.

$$\mu_{tot} = (\mu_x^2 + \mu_y^2 + \mu_z^2)^{1/2} \qquad \text{Eq. 6}$$

$$\langle\alpha\rangle = \frac{1}{3}(\alpha_{xx} + \alpha_{yy} + \alpha_{zz}) \qquad \text{Eq. 7}$$

$$\Delta\alpha = \frac{1}{\sqrt{2}}[(\alpha_{xx} - \alpha_{yy})^2 + (\alpha_{yy} - \alpha_{zz})^2 + (\alpha_{zz} - \alpha_{xx})^2 + 6(\alpha_{xy}^2 + \alpha_{xz}^2 + \alpha_{yz}^2)]^{1/2} \qquad \text{Eq. 8}$$

$$\beta\text{-v} = [(\beta_{xxx} + \beta_{xyy} + \beta_{xzz})^2 + (\beta_{yyy} + \beta_{yzz} + \beta_{yxx})^2 + (\beta_{zzz} + \beta_{zxx} + \beta_{zyy})^2]^{1/2} \qquad \text{Eq. 9}$$

These present components indicate the non-uniform charge distribution along three magnitude. The total dipole moment (μ_{tot}) of **1A** with D-π-D is found to be 2.68 which is the least compared to the chalcone derivatives with D-π-A characteristic [49, 50]. Moreover, the mean polarizability (<α>) of **4EPC** revealed to be 2.13 x 10^{-23} (esu) while the anisotropy of polarizability (Δα) for **4EPC** is 7.51 x 10^{-24} (esu). In addition, the 1st order hyperpolarizability (β-v) of **4EPC** is 1.27 x 10^{-30} (esu) about 2 times higher than standard reference of urea. However, the 1st order hyperpolarizability value of **1A** featuring D-π-D is of the weakest compared to other reported chalcone derivatives due to the attachments of long alkoxy substituted chain which contributed to the long-range charge transfer and might be due to the less conjugation involved throughout molecule. The polarizabilities and first-order hyperpolarizabilities are recorded in atomic units (a.u.), the calculated values have been converted into electrostatic units (esu) using conversion factor of 0.1482 × 10^{-24} esu for α and 8.6393 × 10^{-33} esu for β. Thus, the title compound **4EPC** has an ideal characteristic in potentially to be further taken as candidate in NLO application.

Table 8 Static dipole moments, polarizability and 1st order hyperpolarizability components of title compound **4EPC** with B3LYP/6-31G (d, p) level of theory.

Dipole moment (Debye)	**4EPC**
μ_x	0.8675
μ_y	-2.5257
μ_z	-0.2361
μ_{tot}	2.68
Polarizability	
α_{xx}	-112.2849
α_{yy}	-158.2421
α_{zz}	-160.1713
α_{xy}	10.9656
α_{xz}	0.6285
α_{yz}	0.3233
<α> (x 10^{-24}) in esu	-2.13
Δα (x 10^{-24}) in esu	7.51
1st Hyperpolarizability	
β_{xxx}	-165.3517
β_{xyy}	-5.5160
β_{xzz}	31.8725
β_{yyy}	-24.2823
β_{xxy}	-23.0872
β_{yzz}	0.6083
β_{zzz}	2.5437
β_{xxz}	-2.9405
β_{yyz}	-2.7954
β_{xyz}	-5.7185
β-v (x 10^{-30}) in esu	1.27

ACCEPTED MANUSCRIPT

Conclusions

New alkoxy substituted chalcone derivative (**4EPC**) of D-π-D was successfully synthesized and characterized using FT-IR, ^{1}H and ^{13}C NMR, both UV-vis and TD-DFT for electronic transition characteristics and the crystal structure of **4EPC** was confirmed by single crystal X-ray diffraction method. The crystallographic data indicate that **4EPC** crystallized in monoclinic crystal system with space group *C*2/*c*. The experimental UV-vis spectrum of **4EPC** was performed in a dichloromethane (DCM) and compared with calculated one *via* IEF-PCM model using TD-DFT B3LYP 6-31G (d, p) level of theory. The results obtained were compliment to the experimental findings. The absorption band at λ_{max} = 327 nm was assigned to the electronic transition of HOMO → LUMO orbitals corresponding to the predicted bands 313 nm and 343 nm, excitation energies of 3.56 eV and 3.95 eV and oscillator strength of 1.1197 and 0.1213, where the HOMO-LUMO plot indicates the electron charge mobility from phenyl ring, C=C to carbonyl (C=O) functional group. In addition, the global chemical reactivity descriptors (GCRD) were calculated using frontier molecular orbital energies. From TGA/DTG graph, **4EPC** crystal is thermally stable up to 276 °C with mass loss of 95.2% in single step of degradation process. The Hirshfeld surface analysis and finger print plots were examined to understand the occurrence of molecular interaction within the molecule. Results obtained from Hirshfeld indicated that H···H (65.3%) and C···H (13.5%) interactions are the major contributor in the crystal packing. The MEP analysis revealed the possible interaction can occur at C=O site of the molecule for nucleophilic analyte addition. Since the synthesised chalcone derivative of **4EPC** exhibits larger NLO values in term of polarizability and 1st order hyperpolarizability compared to the standard reference of reported urea, therefore **4EPC** fits all the requirements to be an ideal candidate to be developed as advanced NLO materials. By having excellent NLO properties, **4EPC** also can be an active layer in organic light emitting diode (OLED). Interestingly, from theoretical calculation of **4EPC**, the findings showed that this chalcone derivative is found to be a soft material which having high potential as active materials to be used in pharmaceutical, biological and medicinal interests.

Acknowledgements

ACCEPTED MANUSCRIPT

The authors would like to acknowledge the financial support from Ministry of Education, Malaysia for Fundamental Research Grant Scheme FRGS 59515 (FRGS/1/2018/STG07/UMT/02/6), SLAB/SLAI and Universiti Malaysia Perlis (UniMAP) for postgraduate scholarship, Institute of Marine Biotechnology for NMR analysis and Universiti Malaysia Terengganu for research facilities and supports.

References

1. G. Di Carlo, N. Mascolo, A. A. Izzo, F. Capasso, Flavonoids: old and new aspects of a class of natural therapeutic drugs. Life sciences, 65(4) (1999) 337-353.

2. P. Gunter, (Ed.), Nonlinear Optical Effects and Materials (2000) Springer.

3. P.N. Prasad, D. J. Williams, Introduction to Nonlinear Optical Effects in Molecules and Polymers, Wiley (1991) New York.

4. P. Singh, A. Anand, V. Kumar, Recent developments in biological activities of chalcones: A mini review. Eur. J. Med. Chem. 85 (2014) 758-777.

5. J. Sun, G. Wang, C. Liu, Y. Shi, M. Zhao, Synthesis of four pyrene-containing chalcone derivatives: Achieving excellent third-order nonlinear optical properties by optimizing halopyridines. Opt. Laser Technol. 109 (2019) 600-607.

6. S. Yazıcı, Ç. Albayrak, İ. E. Gümrükçüoğlu, İ. Şenel, O. Büyükgüngör, Experimental and quantum chemical computational study of (E)-1-[5-(3, 4-dimethylphenyldiazenyl)-2-hydroxyphenyl] ethanone. Spectrochim. Acta A. 93 (2012) 208-213.

7. P. S. Patil, S. R. Maidur, M. Shkir, S. AlFaify, V. Ganesh, K. N. Krishnakanth, S. V. Rao, Crystal growth and characterization of second-and third-order nonlinear optical chalcone derivative: (2E)-3-(5-bromo-2-thienyl)-1-(4-nitrophenyl) prop-2-en-1-one. J. Appl. Crystallogr. 51(4) (2018) 1035-1042.

8. D. Coskun, B. Gunduz, M. F. Coskun, Synthesis, characterization and significant optoelectronic parameters of 1-(7-methoxy-1-benzofuran-2-yl) substituted chalcone derivatives. J. Mol. Struct. 1178 (2019) 261-267.

9. S. Muhammad, A. G. Al-Sehemi, M. Pannipara, A. Irfan, A. Design, characterization and nonlinear optical properties of coumarin appended chalcones: Use of a dual approach. Optik. 164 (2018) 5-15.

10. K. H. Ibnaouf, A. O. Elzupir, M. S. AlSalhi, A. S. Alaamer, A. S. Influence of functional groups on the photophysical properties of dimethylamino chalcones as laser dyes. Opt. Mater. 76 (2018) 216-221.

11. Y. Sun, H. Chen, D. Cao, Z. Liu, H. Chen, Y. Deng, Q. Fang, Chalcone derivatives as fluorescence turn-on chemosensors for cyanide anions. J. Photoch. Photobio A. 244 (2012) 65-70.

12. A. R. Chaudhry, A. Irfan, S. Muhammad, A. G. Al-Sehemi, R. Ahmed, Z. Jingping, Computational study of structural, optoelectronic and nonlinear optical properties of dynamic solid-state chalcone derivatives. J. Mol. Graph Model. 75 (2017) 355-364.

13. F. Özen, A. Günel, A. Baran, DNA-binding, enzyme inhibition, and photochemical properties of chalcone-containing metallophthalocyanine compounds. Bioorg. Chem. 81 (2018) 71-78.

14. T. B. Fogaça, R. M. Martins, K. R. Begnini, C. Carapina, M. Ritter, C. M. de Pereira, K. F. Seixas, T. Collares, Apoptotic effect of chalcone derivatives of 2-acetylthiophene in human breast cancer cells. Pharmacol. Rep. 69(1) (2017) 156-161.

15. P. Krawczyk, P. Czeleń, B. Szefler, P. Cysewski, P. Theoretical studies on the interaction between chalcone dyes and Concanavalin A—The reactive group effects on the photophysical and biological properties of the fluorescence probe. J. Photoch. Photobio A. 346 (2017) 327-337.

16. H. Kantekin, H. Yalazan, N. Kahriman, B. Ertem, V. Serdaroğlu, M. Pişkin, M. Durmuş, New peripherally and non-peripherally tetra-substituted metal-free, magnesium (II) and zinc (II) phthalocyanine derivatives fused chalcone units: Design, synthesis, spectroscopic characterization, photochemistry and photophysics. J. Photoch. Photobio A. 361 (2018) 1-11.

17. S. Balamurugan, S. Nithyanandan, C. Selvarasu, G. Y. Yeap, P. Kannan, P. Photophysical and photochemical investigations on triazole ring linked chalcone containing polymethacrylates. Polymer. 53(19) (2012) 4104-4111.

18. C. G. Niu, A. L. Guan, G. M. Zeng, Y. G. Liu, Z. W. Fluorescence water sensor based on covalent immobilization of chalcone derivative. Anal. Chim. Acta. 577(2) (2006) 264-270.

19. S. Kar, K. S. Adithya, P. Shankar, N. J. Babu, S. Srivastava, G. N. Rao, Nonlinear optical studies and structure-activity relationship of chalcone derivatives with in silico insights. J. Mol. Struct. 1139 (2017) 294-302.

20. A. R. Chaudhry, A. Irfan, S. Muhammad, A. G. Al-Sehemi, R. Ahmed, Z. Jingping, Computational study of structural, optoelectronic and nonlinear optical properties of dynamic solid-state chalcone derivatives. J. Mol. Graph. Model. 75 (2017) 355-364.

21. M. M. Makhlouf, A. S. Radwan, B. Ghazal, Experimental and DFT insights into molecular structure and optical properties of new chalcones as promising photosensitizers towards solar cell applications. Appl. Surf. Sci. 452 (2018) 337-351.

22. P. Rajakumar, A. Thirunarayanan, S. Raja, S. Ganesan, P. Maruthamuthu, Photophysical properties and dye-sensitized solar cell studies on thiadiazole–triazole–chalcone dendrimers. Tetrahedron Lett. 53(9) (2012) 1139-1143.

ACCEPTED MANUSCRIPT

23. S. R. Prabhu, A. Jayarama, K. Chandrasekharan, V. Upadhyaya, S. W. Ng, Synthesis, growth, structural characterization, Hirshfeld analysis and nonlinear optical studies of a methyl substituted chalcone. J. Mol. Struct. 1136 (2017) 244-252.

24. B. Deepa, P. Philominathan, Investigation on the optical, mechanical and magnetic properties of organic NLO single crystal: Pyridine 3-carboxylic acid. Optik-Int. J. Light. Elect. Opt. 127(20) (2016) 8698-8705.

25. M. Rajkumar, A. Chandramohan, Synthesis, spectral, thermal, mechanical and structural characterization of NLO active organic salt crystal: 3, 5-Dimethylpyrazolium-3-Nitrophthalate. Mater. Lett. 181 (2016) 354-357.

26. V. Shettigar, P. S. Patil, S. Naveen, S. M. Dharmaprakash, M. A. Sridhar, J. S. Prasad, Crystal growth and characterization of new nonlinear optical chalcone derivative: 1-(4-Methoxyphenyl)-3-(3, 4-dimethoxyphenyl)-2-propen-1-one. J. Cryst. Growth. 295(1) (2006) 44-49.

27. F. Z. Henari, D. Gaynor, D. M. Griffith, C. M. Mulcahy, C. J. Marmion, Non-linear optical measurement of Iron (III) Tris (pyridinehydroxamate) complexes. Chem. Phys. Lett. 552 (2012) 126-129.

28. D. R. Kanis, M. A. Ratner, T. J. Marks, Design and construction of molecular assemblies with large second-order optical nonlinearities. Quantum chemical aspects. Chemical Reviews, 94(1) (1994) 195-242.

29. S. Y. Kim, M. Lee, B. H. Boo, Second molecular hyperpolarizability of 2, 2′-diamino-7, 7′-dinitro-9, 9′-spirobifluorene: An experimental study on third-order nonlinear optical properties of a spiroconjugated dimer. J. Chem. Phys. 109(7) (1998) 2593-2595.

30. W. M. Khairul, A. I. Daud, N. A. M. Hanifaah, S. Arshad, I. A. Razak, H. M. Zuki, M. F. Erben, Structural study of a novel acetylide-thiourea derivative and its evaluation as a detector of benzene. J. Mol. Struct. 1139 (2017) 353-361.

31. A.I. Daud, W. M. Khairul, H. M. Zuki, K. Kubulat, Aerobic synthetic approach and characterisation of some acetylide–thiourea derivatives for the detection of carbon monoxide (CO) gas. J. Mol. Struct., 1093 (2015) 172-178.

32. A. I. Daud, W. M. Khairul, K. A. A. Wahid, Organic Semiconductor Material Featuring 4-Ethylbenzoyl-3-(4-ethynylbenzonitrile-phenyl)-thiourea (CYT-1) of Donor-π-acceptor for Chemiresistive Carbon Dioxide (CO_2) Sensing. J. Phys. Sci. 29 (2018) 75-81.

33. Bruker SADABS, APEX2 and SAINT. Bruker AXS Inc Madison WI, USA, 2009.

34. G. M. Sheldrick, A short history of SHELX. Acta. Cryst. A. 64(1) (2008) 112-122.

35. G. M. Sheldrick, Crystal structure refinement with SHELXL. Acta. Cryst. C. 71(1) (2015) 3-8.

36. A. L. Spek, Structure validation in chemical crystallography. Acta. Cryst. D. 65(2) (2009) 148-155.

37. C. F. Macrae, P. R. Edgington, P. McCabe, E. Pidcock, G. P. Shields, R. Taylor, J. V. D. Streek, Mercury: visualization and analysis of crystal structures. J. App. Cryst. 39(3) (2006) 453-457.

38. M. J. Frisch, G. W. Trucks, H. B. Schlegel, G. E. Scuseria, M. A. Robb, J. R. Cheeseman, G. Scalmani, V. Barone, G. A. Petersson, H. Nakatsuji, X. Li, M. Caricato, A. V. Marenich, J. Bloino, B. G. Janesko, R. Gomperts, B. Mennucci, H. P. Hratchian, J. V. Ortiz, A. F. Izmaylov, J. L. Sonnenberg, D. Williams-Young, F. Ding, F. Lipparini, F. Egidi, J. Goings, B. Peng, A. Petrone, T. Henderson, D. Ranasinghe, V. G. Zakrzewski, J. Gao, N. Rega, G. Zheng, W. Liang, M. Hada, M. Ehara, K. Toyota, R. Fukuda, J. Hasegawa, M. Ishida, T. Nakajima, Y. Honda, O. Kitao, H. Nakai, T. Vreven, K. Throssell, J. A. Montgomery, J. E. Peralta, F. Ogliaro, M. J. Bearpark, J. J. Heyd, E. N. Brothers, K. N. Kudin, V. N. Staroverov, T. A. Keith, R. Kobayashi, J. Normand, K. Raghavachari, A. P. Rendell, J. C. Burant, S. S. Iyengar, J. Tomasi, M. Cossi, J. M. Millam, M. Klene, C. Adamo, R. Cammi, J. W. Ochterski, R. L. Martin, K. Morokuma, O. Farkas, J. B. Foresman, D. C. Fox, Gaussian, Inc., Wallingford CT, 2016.

39. R. Dennington, Keith, A. Todd, J. M. Millam, Semichem Inc., Shawnee Mission, KS, 2016.

40. B. B. Jain, R. B. Patel, Synthesis, Characterization and Mesomorphic Study of new Homologous Chalcone Series. World Scientific News, 3(53) (2016) 241-252.

41. S. R. Prabhu, V. Upadhyaya, A. Jayarama, Synthesis, crystal structure and Hirshfeld surface analysis of a novel chalcone derivative: (2E)-3-(2, 3-dimethoxyphenyl)-1-(3-nitrophenyl) prop-2-en-1-one. Chem. Data Collect. 11 (2017)199-210.

42. H. C. Kwong, M. S. Rakesh, C. C. Kumar, S. R. Maidur, P. S. Patil, C. K. Quah, Y. F. Win, C. Parlak, S. Chandraju, S. Structure–property relation and third-order nonlinear optical studies of two new halogenated chalcones. Zeitschrift für Kristallographie-Cryst. Mater. 233(5) (2018) 349-360.

43. H. Kagawa, M. Sagawa, A. Kakuta, A. 3-(4-tert-Butylphenyl)-3-hydroxy-1-(4-methoxyphenyl)-2-propen-1-one: an SHG active β-diketone. Acta. Cryst. C. 49(12) (1993) 2181-2183.

44. P. T. Mahadeva, S. MA, P. J. Shashidhara, Synthesis and Crystal Structure of 3-(4-Ethylphenyl)-1-(2-hydroxy-4-methoxyphenyl) prop-2-en-1-one. X-ray Structure Analysis Online, 27 (2011) 39-40.

45. K. Kumara, M. Jyothi, N. Shivalingegowda, S. A. Khanum, L. N. Krishnappagowda, L. Synthesis, characterization, crystal structure and Hirshfeld surface analysis of 1-(4-ethoxyphenyl)-3-(4-methylphenyl) prop-2en-1-one. Chem. Data. Collect. 9 (2017) 152-163.

ACCEPTED MANUSCRIPT

46. J. Bernstein, R. E. Davis, L. Shimoni, N. L. Chang, Patterns in hydrogen bonding: functionality and graph set analysis in crystals. Angewandte Chemie International Edition in English, 34(15) (1995) 1555-1573.

47. S. R. Maidur, J. R. Jahagirdar, P. S. Patil, T. S. Chia, C. K. Quah, Structural characterizations, Hirshfeld surface analyses, and third-order nonlinear optical properties of two novel chalcone derivatives. Opt. Mater. 75 (2018) 580-594.

48. B. Pramodh, N. K. Lokanath, S. Naveen, P. Naresh, S. Ganguly, J. Panda, Molecular structure, Hirshfeld surface analysis, theoretical investigations and nonlinear optical properties of a novel crystalline chalcone derivative:(E)-1-(5-bromothiophen-2-yl)-3-(p-tolyl) prop-2-en-1-one. J. Mol. Struct. 1161 (2018) 9-17.

49. P. S. Patil, M. Shkir, S. R. Maidur, S. AlFaify, M. Arora, S. V. Rao, H. Abbas, V. Ganesh, Key functions analysis of a novel nonlinear optical D-π-A bridge type (2E)-3-(4-Methylphenyl)-1-(3-nitrophenyl) prop-2-en-1-one chalcone: an experimental and theoretical approach. Opt. Mater. 72 (2017) 427-435.

50. M. N. Arshad, A. A. M. Al-Dies, A. M. Asiri, M. Khalid, A. S. Birinji, K. A. Al-Amry, A. A. Braga, Synthesis, crystal structures, spectroscopic and nonlinear optical properties of chalcone derivatives: a combined experimental and theoretical study. J. Mol. Struct. 1141 (2017) 142-156.

ACCEPTED MANUSCRIPT

ACCEPTED MANUSCRIPT

RESEARCH HIGHLIGHTS

- A new class of chalcone derivative of alkoxy-chalcone was designed and prepared.
- Its electronic properties exhibited organic semiconductor behavior.
- Interestingly, the single crystal possesses heart-shape motif.

ACCEPTED MANUSCRIPT